

# Effective Lymph Nodes Detection in CT Scans Using Location Debaised Query Selection and Contrastive Query Representation in Transformer

Yirui Wang<sup>1\*</sup>, Qinji Yu<sup>1,2\*</sup>, Ke Yan<sup>2,3</sup>, Haoshen Li<sup>4</sup>, Dazhou Guo<sup>2</sup>,  
Li Zhang<sup>4</sup>, Na Shen<sup>5</sup>, Qifeng Wang<sup>6</sup>, Xiaowei Ding<sup>1</sup>, Le Lu<sup>2</sup>, Xianghua Ye<sup>7</sup>,  
and Dakai Jin<sup>2</sup>

<sup>1</sup>DAMO Academy, Alibaba Group. <sup>2</sup>Shanghai Jiao Tong University.

<sup>3</sup>Hupan Lab, 310023, Hangzhou, China. <sup>4</sup>Peking University.

<sup>5</sup>Zhongshan Hospital Fudan University. <sup>6</sup>Sichuan Cancer Hospital.

<sup>7</sup>The First Affiliated Hospital Zhejiang University.

{yirui.wang, dakai.jin}@alibaba-inc.com, hye1982@zju.edu.cn

**Abstract.** Lymph node (LN) assessment is a critical yet very challenging task in the routine clinical workflow of radiology and oncology. Accurate LN analysis is essential for cancer diagnosis, staging and treatment planning. Finding scatteredly distributed, low-contrast clinically relevant LNs in 3D CT is difficult even for experienced physicians under high inter-observer variations. Previous automatic LN detection typically yields limited recall and high false positives (FPs) due to adjacent anatomies with similar image intensities, shapes or textures (vessels, muscles, esophagus, etc). In this work, we propose a new LN DETECTION TRansformer, named LN-DETR, with location debaised query selection and contrastive query learning to enhance the representation ability of LN queries, important to increase the detection sensitivity and reduce FPs or duplicates. We also enhance LN-DETR by adapting an efficient multi-scale 2.5D fusion scheme to incorporate the 3D context. Trained and tested on 3D CT scans of 1067 patients (with 10,000+ labeled LNs) via combining seven LN datasets from different body parts (neck, chest, and abdomen) and pathologies/cancers, our method significantly improves the performance of previous leading methods by  $> 4 \sim 5\%$  average recall at the same FP rates in both internal and external testing. We further evaluate on the universal lesion detection task using DeepLesion benchmark, and our method achieves the top performance of 88.46% averaged recall, compared with other leading reported results.

**Keywords:** CT · Lymph Node Detection · Detection Transformer

## 1 Introduction

Computer-aided detection (CADe) has been an active research area in medical image analysis for the past three decades, evolving rapidly in recent years when

---

\* Equal contribution.

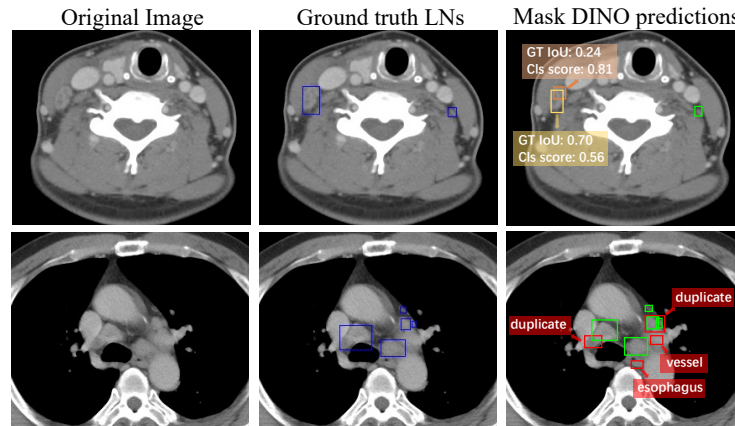


**Fig. 1:** LN detection challenges by the current state-of-the-art detector (*e.g.*, Mask DINO [25]). **Blue, green, and red** boxes denote the ground-truths (GTs), true-positives (TPs), and false-positives (FPs), respectively. The predictions in 1st row show the misalignment between the classification score and the LN box quality (*i.e.*, IoU), while the 2nd row indicates some hard false-positives (FPs) and duplicated predictions.

equipped with deep learning techniques [?, 1, 10, 11, 39, 48]. Among CADe tasks, lymph node (LN) identification is a critical yet under-studied problem, which accounts for a significant part of routine clinical workload for both radiology and oncology [7, 40, 52] clinical problems. As the integral components of human immune system, LNs are broadly distributed throughout whole body along lymphatic pathways, also as the main pathways for cancer spreading. LN assessment is usually using the 3D computed tomography (CT) scan. Therefore, accurate detection of clinically significant LNs in CT is important for cancer diagnosis, staging, treatment planning, and prognosis evaluation [12, 14, 21, 47].

LN detection in CT can be a very challenging clinical task for physicians for several reasons. First, given the indistinguishable intensity of LNs relative to adjacent soft tissues, the relative contrast between LNs and adjacent normal anatomies is very low. Second, besides intensity, LNs also exhibit comparable sizes and shapes (spherical or ellipsoid) with nearby soft tissues. These similarities make LNs being easily confused with vessels, muscles, esophagus, pericardial recesses, and other structures (some examples in Fig. 1). As a result, even for experienced board-certified radiologists, missing or misidentification of LNs might occur. Moreover, LNs are scatteredly distributed in various body regions, such as the neck, axilla, chest, and abdomen. Hence, manual inspection from hundreds of 2D image slices per patient’s CT scan would easily misidentify clinically significant LNs, especially under a time restriction.

Previous works investigate automatic LN detection using hand-crafted features or CNN-based approaches. Conventional statistical learning methods employ hand-crafted image features, such as shape, spatial priors, Haar filters, and volumetric directional difference filters, to capture LNs’ appearance and subse-

quently localize them [2, 16, 33]. CNN-based approaches achieve better performance by applying FCN [35] or Mask R-CNN [18] to directly segment and detect LNs [41, 54, 57]. However, these works only detect the enlarged LNs (short-axis  $\geq 10\text{mm}$ ), despite that enlarged size alone is not a reliable predictive factor for LN malignancy with only 60%-80% sensitivity in lung cancer patients [37, 49]. Recent CNN-related works [5, 59] try to detect both enlarged and smaller LNs using LN station priors (oftentimes not available in clinical practice), yet, low performance is reported ( $< 60\%$  recall in [5]). Another limitation of previous work is that they usually focus on a single body region, such as the chest or abdomen, lacking a universal LN detection model covering all major body sections.

Recently, vision transformers have been widely studied in the computer vision community and remarkable progress has been achieved [6, 9, 13]. For object detection, the seminal work of DEtection TRansformer (DETR) [6] formulates object detection as a set prediction task and assigns labels by bipartite graph matching. DETR-based detection models [24, 34, 65, 69] have demonstrated superior performance compared to CNN-based detectors. Among them, DINO (DETR with Improved deNoising anchOr boxes) [65] achieves the leading performance by improving a denoising training process [24] and utilizing a mixed query selection for anchor initialization. Later, Mask DINO [25] further extends DINO by adding a mask prediction branch to support the segmentation task. Transformer detectors have been rarely explored in CADe [29, 50].

Inspired by the success of DETR-based detectors for objection detection in natural images, here, we address the universal LN detection problem by proposing a new end-to-end LN DEtection TRansformer, named LN-DETR. Built upon Mask DINO [25], LN-DETR inherits the key components of the denoising training and mixed query selection for anchor initialization. Importantly, we further improve LN-DETR based on the following two key observations. (1) CT is volumetric data with important 3D context for LN identification. However, a pure 3D DETR is computationally expensive and cannot utilize pre-trained weights, which is critical for achieving high performance with transformer models. Hence, we first enhance LN-DETR by utilizing an efficient multi-scale 2.5D fusion scheme to incorporate the 3D context while leveraging pre-trained 2D weights. (2) Unlike natural images where objects typically possess distinct edges, in CT scans, LN’s boundary yields subtle differences from adjacent anatomies, exhibiting similar intensities, shapes, or textures. Hence, even the leading detector Mask DINO would generate a large number of false-positives (FPs) or duplicate predictions near true LNs (see 2nd row of Fig. 1).

To address this particular issue, we introduce two main technical developments in LN-DETR aiming to enhance LN’s query embedding quality, which would subsequently improve the localization accuracy and better distinguish true LNs from other similar anatomies (appeared as FPs or duplicate predictions). First, we append an IoU prediction task to estimate the localization confidence of queries. Then, we propose a location debiased query selection to choose LN queries with higher localization confidence. These IoU-enhanced queries serve as the initial content queries and initial anchors for the decoder,

ensuring a more precise decoding initialization. In addition, we introduce a query contrastive learning module at the decoder’s output, which explicitly enhances positive queries towards their best-matched ground-truth (GT) queries over the unmatched negative query predictions. As shown in the ablation study, these two new components significantly improve the quantitative LN detection performance. In summary, our main contributions are as follows:

- We are the first to explore the transformer-based detector to tackle the challenging yet clinically important LN detection task. We collect and curate a large scale of LN CT scans containing 1067 patients (with 10,000+ labeled LNs of both enlarged and small sizes) from 7 clinical institutions across different body parts (neck, chest, and abdomen) and various pathologies.
- We propose a new LN detection transformer, LN-DETR, with location debiased query selection and contrastive query learning to enhance the representation ability of LN queries, important to increase the detection sensitivity and reduce FPs or duplicates. We also enhance LN-DETR by adapting an efficient multi-scale 2.5D fusion scheme to incorporate the 3D context.
- Trained and evaluated on CT scans of 1067 patients, our method significantly improves previous leading detection methods by at least 4 ~ 5% average recall in both internal (5 datasets) validation and external (2 datasets) testing.
- We further evaluate LN-DETR on the universal lesion detection task using NIH DeepLesion dataset [61] and demonstrate its effectiveness by achieving the top performance from quantitative benchmarks.

## 2 Related Work

**Detection transformer:** Early CNN-based object detectors are formulated via either two-stage [18, 46] or one-stage architecture [44, 45] with hand-designed components (anchor boxes and non-maximum suppression), which makes them difficult for end-to-end optimization. The first end-to-end object DETection TRANSformer (DETR) removes these hand-designed components [6]. Follow-up studies [19, 38, 55, 63] attempt to address the slow convergence issue or explore a deeper understanding of decoder queries. Among them, Deformable-DETR predicts 2D anchor points and designs a deformable attention module that only attends to certain sampling points around a reference point [69]. DAB-DETR represents queries as 4D anchor box coordinates to subsequently update boxes in the decoder [34]. DINO (DETR with Improved deNoising anchOr boxes) [65] outperforms CNN-based detectors by a marked margin with an enhanced version for denoising training as an extension to that in DN-DETR [24]. Mask DINO further extends DINO by adding a mask prediction branch supporting different segmentation tasks [25]. Our LN-DETR model is built upon Mask DINO and we make several key contributions to improve the performance in LN detection.

**Misaligned classification and localization confidence:** The majority of CNN detectors [32, 46, 53] only adopt classification confidence as the criterion for ranking proposal boxes during the non-maximum suppression (NMS) post-processing. However, this method neglects the localization quality of proposals

since classification confidence does not necessarily correlate with localization accuracy. To address this misalignment issue, [20, 28] introduce auxiliary IoU estimators, considering both classification and localization accuracy in the NMS process. [30, 67] incorporate variations of focal loss to learn a joint representation of object confidence and localization quality, improving the ranking of proposal boxes during NMS. The misalignment of classification and localization confidence has also been observed in DETR-based methods [43, 64]. An IoU-aware query recalibration module is proposed to estimate an extra IoU score and use it to calibrate the decoder query’s confidence that better reflects the quality of predictions [64]. Nevertheless, recalibration is limited to the decoding stage, and our experiments reveal that this may cause sub-optimal detection performance. Here, we explicitly debias query’s box content at encoder’s output, ensuring a more precise decoding initialization and improving the performance.

**LN detection and segmentation:** Automatic LN detection has been exploited by focusing on extracting effective LN features, incorporating organ priors, or utilizing advanced learning models. Early works often adopt the model-based or statistical learning-based methods [2, 15, 16, 33]. CNN-based approaches have recently been explored [36, 54, 56]. Mask R-CNN is improved with a global-local attention module and a multi-task uncertainty loss to detect LNs in abdomen MR images [54]. Another line of work explores various CNN-based segmentation models for LN detection [5, 17, 41, 70, 71]. However, segmentation based methods often require additional labels (*e.g.*, annotating organ or LN station masks) [5, 17] or imaging modality (*e.g.*, PET) [?, 70], narrowing their applicability in clinical use. Moreover, directly segmenting LNs may not be optimal, since LNs are small and scatteredly distributed objects, where voxel-wise segmentation loss can be difficult to supervise the instance-oriented target learning. Previous work usually focus on a single body region/disease, or only detect enlarged LNs (size  $\geq 10\text{mm}$ ) disregarding smaller metastatic LNs that are yet clinically critical. To the best of our knowledge, we are the first to detect both enlarged and smaller LNs on a large-scale dataset (1000+ patients) across different body parts and various diseases, as a notably more challenging technical and clinical task.

### 3 Method

In this section, we first provide an overview of the architecture of LN-DETR in Sec. 3.1. Then, the location debiased query selection is introduced in Sec. 3.2 to solve the bias issue when selecting anchor proposals and producing final predictions. Lastly, we elaborate query contrastive learning modules in Sec. 3.3 to eliminate low-quality predictions.

#### 3.1 LN-DETR Architecture

Fig. 2 depicts the proposed LN-DETR framework, which consists of a CNN backbone with multi-scale 2.5D feature fusion and transformer encoder and decoder. We elaborate on each component below.

**Multi-scale 2.5D feature fusion:** While 3D context is essential for LN detection in CT scans, 3D detectors usually yield inferior performance to 2D models initialized with pre-trained weights by large-scale training data. To bridge this gap, we adapt a 2.5D feature level fusion scheme [60] to our LN-DETR. Different from [60] that only uses outputs of FPN for predictions, we feed the 2.5D fused features from multiple levels (as illustrated in Fig. 2) to the transformer encoder to avoid information loss and enable the cross-scale token interactions in encoder layers. This fusion operation is applied to all four ResNet blocks. Other 2.5D fusion methods can also be possibly adapted to LN-DETR, and the comparison of different 2.5D strategies is beyond the scope of this work.

**Detection transformer:** The overall architecture of LN-DETR is similar to Mask DINO [25]. Compared to the original DETR [6], Mask DINO adopts a multi-scale deformable attention module [69] to aggregate multi-scale feature maps. Additional denoising queries and denoising losses are implemented to accelerate the training convergence. Moreover, it computes top-scoring queries (used as region proposals) from the output of the transformer encoder to initialize the content queries and reference boxes that are fed into the decoder for subsequent refinement. For selecting the top  $K$  queries, only classification confidence is considered as the ranking criterion for selecting both decoder reference anchor boxes and final top predictions, leading to *biased* box predictions that may lean to high object confidence but without considering localization accuracy.

### 3.2 Location Debaised Query Selection

**Biased criterion and prior solutions:** As shown in the 1st row of Fig. 1, predicted LN bounding boxes with higher classification confidences paradoxically exhibit smaller overlaps with the corresponding GT boxes. This illustrates that classification confidence may not positively related to the quality of predicted bounding boxes. As a result, using such location biased selection criterion may lead to sub-optimal predictions from the decoder. In addition, state-of-the-art DETR detectors are typically formulated as a two-stage method (denoted as  $\hat{b} = b_{ref} + \Delta b$ ), where the encoder generates reference anchor boxes ( $b_{ref}$ ) that are then iteratively refined by the decoder ( $\Delta b$ ). Under such setting, [64] solves this bias issue by appending an IoU prediction head in parallel with the classification head in the decoder and jointly selecting the final query box predictions  $\hat{b}$ . Nevertheless, [64] only focuses on the final results and neglects the accuracy of intermediate results (*i.e.*, encoder anchor predictions  $b_{ref}$ ), leading to the degraded decoder anchor initialization and sub-optimal box refinement.

Partially inspired but different from [64], we propose debaised query selection to explicitly optimize encoder anchors  $b_{ref}$  and decoder refinement  $\Delta b$  simultaneously, ensuring a location-enhanced anchor initialization for the decoder and producing the optimal refined final predictions. The debaised query selection also addresses the issue of sub-optimal bounding boxes optimization in DETR/Mask DINO, which arises when a predicted box has a high-class score but erroneously includes surrounding anatomies that are easily confused with LNs. This leads to

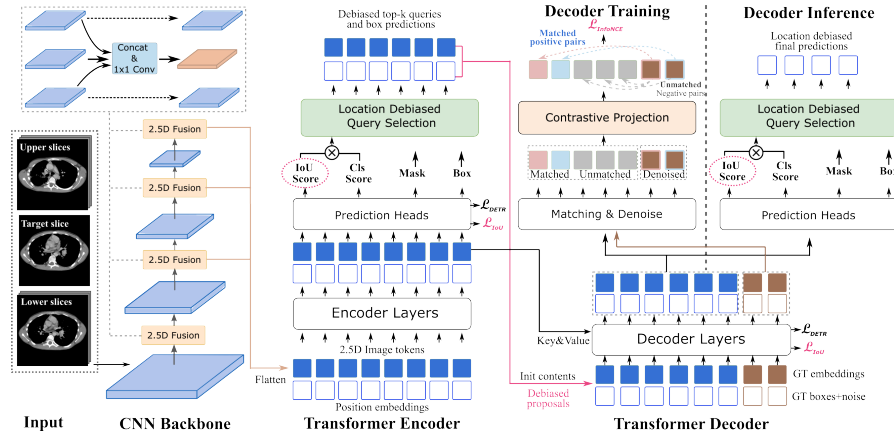


**Fig. 2:** Overall framework of our proposed LN-DETR, composed of a CNN backbone with multi-scale 2.5D feature fusion and a transformer encoder and decoder. Our improvements include location debaised query selection module in both encoder and decoder, and a query contrastive learning module on improving query representation ability to distinguish true LN queries from nearby FPs or duplicate queries.

the parameters being updated to falsely identify these representations as characteristic features of LNs, resulting in duplicates and FPs. Debiased query selection recalibrates the selection criteria by considering both classification and localization accuracy to sufficiently address this ambiguity.

**Query debiasing procedure:** To select queries with both high classification and localization accuracy, we first train an additional IoU prediction head. As the pink dotted circle shown in Fig. 2, an IoU prediction heads are introduced at the last layer of the transformer encoder and all decoder layers (parameters shared across layers) to predict the localization accuracy (IoU) for queries. The IoU prediction head consists of a single MLP layer in parallel to the classification, box regression, and mask generation heads. Note that we only train the IoU prediction head for the *matched* queries after the bipartite matching [23]. To train the IoU prediction head, we supervise the IoU predictions with the true IoU values between the GTs and the *matched* box predictions. Given a CT slice with  $M$  GT boxes, we denote the matched  $M$  query features as  $\{q_1, q_2, \dots, q_M\}$  and the IoU prediction for each query as  $\text{IoU}_q^P$ . Suppose that the Hungarian Matching assigns the  $i$ -th GT to the  $j$ -th query, then we can calculate the IoU score of the query’s box prediction to the matched GT box, denoted  $\text{IoU}_{q_j}^{\text{GT}_i}$ . The IoU loss for the  $i$ -th GT is defined as,

$$\mathcal{L}_{\text{IoU}} = \left\| \text{IoU}_{q_j}^P - \text{IoU}_{q_j}^{\text{GT}_i} \right\|^2 \quad (1)$$

With the computed IoU prediction (as localization confidence), we use a new query ranking score by simply multiplying the query’s IoU score with its classification score. We select the top  $K$  queries based on the new score (more accurate

LN bounding boxes) at the output of the encoder. During inference, we also apply this query debiasing procedure at the last decoder layer to select the best refined box predictions.

### 3.3 Query Contrastive Learning

Another observed issue in LN detection is that DETR/Mask DINO often contains duplicates or false positives due to the vagueness of LN boundaries with the adjacent visually similar anatomies (see 2nd row of Fig. 1). We argue that the main reason may be due to the one-to-one matching step by Hungarian algorithm [23], which only assigns each GT to its best matched query and forces all unmatched queries to predict the same background label by solely using the CE loss without considering their relative ranking. This leads to insufficient and ambiguous supervision to discriminate locally similar queries. Moreover, a previous study [22] highlights the limitations of optimizing CE loss alone (vulnerability to noisy labels and poor class margins). It also shows that contrastive learning is capable of performing hard negative mining. To alleviate this issue, we introduce a simple yet effective approach to better distinguish LNs from similar adjacent anatomies or duplicate predictions at the feature level by adding a query contrastive learning module (naturally utilizing the denoising anchor boxes in Mask DINO) at the output of the decoder. The construction of positive and negative query pairs and the detailed computation process are described below.

**Constructing positive and negative query pairs:** An intuitive way to construct the positive and negative query pair is to use the Hungarian matching results: each GT and its best-matched output query form a positive pair, while all other unmatched queries of this GT serve as negative ones. In this setting, GT needs to have its query representation, *e.g.*, it can be derived by processing the GT box and label embedding through the transformer decoder. Fortunately, GT-query can be readily acquired by the denoising training process in Mask DINO. Utilizing the multi-group denoising training [25], we obtain multiple GT-queries corresponding to the same GT to form multiple positive pairs, which encourages more divergence and robustness further benefiting the contrastive learning. Specifically, assume that we have  $N$  denoising groups, and each group contains  $M$  denoised GT-queries, *i.e.*, anchor queries, thus the total anchor queries  $\mathbf{q}^{\text{DN}}$  are

$$\mathbf{q}^{\text{DN}} = \left\{ \begin{array}{ccc} q_{11}^{\text{DN}} & \cdots & q_{1N}^{\text{DN}} \\ \vdots & \ddots & \vdots \\ q_{M1}^{\text{DN}} & \cdots & q_{MN}^{\text{DN}} \end{array} \right\}_{M \times N}, \quad (2)$$

where  $M$  is the number of GT LN boxes in the CT slice. Suppose the  $k$ -th query has the minimal matching cost with the  $i$ -th GT in the CT slice, then,  $q_k$  is the positive query paired with  $N$  anchor queries  $q_i^{\text{DN}}$ , and other unmatched  $K - 1$  queries are treated as negative queries for  $q_i^{\text{DN}}$ .

**Contrastive computation:** Instead of directly measuring the similarity between different query embeddings, we first project query embeddings into a latent space using a simple shared MLP layer  $\phi$  [8]. With the projected query

embeddings, similarities between all positive-anchor and negative-anchor pairs are computed and the InfoNCE loss [42] is adopted to pull the matched positive query close to its assigned anchor query while pushing away from all other unmatched negative ones. The total query contrastive loss for the given CT slice is formulated as

$$\mathcal{L}_{\text{InfoNCE}} = - \sum_{i=1}^M \sum_{j=1}^N \log \left[ \frac{e^{\langle \phi(q_k), \phi(q_{ij}^{\text{DN}}) \rangle / \tau}}{\sum_{k'=1}^K e^{\langle \phi(q_{k'}), \phi(q_{ij}^{\text{DN}}) \rangle / \tau}} \right] \quad (3)$$

where  $\langle \cdot, \cdot \rangle$  is the cosine similarity, and  $\tau$  is the temperature coefficient, which is set to 0.05. We apply this contrast loss for the output queries of the last decoder layer. We only employ the contrastive learning scheme during training and remove it when performing inference.

**Training objective function:** In training, the total loss function combines all above losses, *i.e.*, classification, box regression, and mask losses, and the proposed IoU prediction loss and query contrastive loss,

$$\mathcal{L}_{\text{total}} = \lambda_1 \mathcal{L}_{\text{cls}} + \lambda_2 \mathcal{L}_{\text{box}} + \lambda_3 \mathcal{L}_{\text{mask}} + \lambda_4 \mathcal{L}_{\text{IoU}} + \lambda_5 \mathcal{L}_{\text{InfoNCE}} \quad (4)$$

where  $\lambda_{1-5}$  are the weights for each loss component, and we keep  $\lambda_{1-3}$  the same as the original Mask DINO work, and set  $\lambda_4 = 10, \lambda_5 = 1$  according to our experiments.

## 4 Experiments

We first evaluate our LN-DETR model in LN detection task and seven LN datasets of different body parts and diseases are collected with a total of 1067 patients with 10,000+ labeled LN instances. Among them, five datasets are used for model development and internal testing and the rest two are kept as independent external testing. Leading CNN- and transformer-based detection and segmentation methods are compared. To further demonstrate the effectiveness and generalizability of LN-DETR, we report quantitative universal lesion detection results and comparisons, trained and evaluated on NIH DeepLesion dataset [61].

### 4.1 Datasets and Evaluation Metrics

**LN datasets:** Seven LN datasets are collected and curated including 1067 patients with 10,000+ annotated LNs containing various body parts (neck, chest, and upper abdomen) and different diseases (head & neck cancer, esophageal cancer, lung cancer, COVID, and other diseases), which will be public available for download <sup>1</sup>. The detailed patient number, LN number, imaging protocol, and evaluation setting are summarized in Table 1. While NIH-LN [5] is a public LN dataset, the rest six datasets are collected from five clinical centers. We use NIH-LN and 4 datasets from Center 1-3 (covering head & neck, esophageal and

<sup>1</sup> [https://github.com/CSCYQJ/ECCV24\\_LN\\_DETR](https://github.com/CSCYQJ/ECCV24_LN_DETR)

**Table 1:** Statistics of 7 LN detection datasets, where 5 of them are used as the internal data for the model development and internal testing and the rest 2 are used as independent external testing set. NIH-LN is a public dataset, and other datasets are in-house datasets collected from five different clinical centers. HN, Eso and Mul. represent head & neck cancer, esophageal cancer and multiple types of diseases, respectively.

Dataset	#Patient	#LNs	Avg. Res. (mm)	Body Parts	Setting
NIH-LN	89	1956	(0.82, 0.82, 2.0)	chest & abdomen	internal
Center1-HN	256	1890	(0.46, 0.46, 4.0)	head & neck	
Center2-Eso	91	857	(0.70, 0.70, 4.9)	chest	
Center2-Lung	97	668	(0.71, 0.71, 5.0)	chest	
Center3-Eso	300	2515	(0.85, 0.85, 5.0)	chest	
Center4-Mul	184	2131	(0.76, 0.76, 2.0)	chest & abdomen	external
Center5-HN	50	418	(0.48, 0.48, 1.2)	head & neck	
Total	1067	10435	-	-	-

lung cancers) as the **internal dataset** to develop and internally test the model performance. Datasets from Center4 and 5 are used as **independent external testing set**, where Center4-Mul. contains three different types of patients, *i.e.*, lung cancer, esophageal cancer, and infectious lung disease. For the five internal datasets, we randomly split each dataset into 70% training, 10% validation, and 20% testing at the patient level. Training and validation data from the five datasets are used together to develop and select the LN detection model, and rest testing patients from the five datasets are reserved to report the internal testing results.

**Universal lesion datasets:** NIH DeepLesion consists of 32, 735 lesions from 4427 patients. It contains a variety of lesions including lung nodules, liver/kidney/bone lesions, enlarged LNs, and so on. We use the official training/validation/test split and report results on the test set.

**Evaluation metrics:** For LN detection, following previous works [4, 58, 60], we use the free-response receiver operating characteristic (FROC) curve as the evaluation metric and report the sensitivity/recall at 0.5, 1, 2, 4 FPs per patient/CT-volume. We merge 2D detection boxes of all methods to 3D ones following [54, 58]. When comparing a detected 3D box with the GT 3D box, a predicted box is considered as true positive if its 3D intersection over the detected bounding-box ratio (IoBB) is larger than 0.3 [58]. We also report average precision (AP) at 0.1 IoU threshold in 3D by following [3]. For lymph node detection, as metastatic LNs can be as small as 5mm, we set a post-processing size threshold of 5mm to detect both enlarged and smaller LNs (short axis  $\geq$  5mm) during inference. If a GT LN smaller than 5mm is detected, it is neither counted as a TP nor an FP. In training, we use LN annotations of all sizes.

For DeepLesion detection, we use its official evaluation metrics, *i.e.*, sensitivity/recall at 0.5, 1, 2, 4 FPs per image/CT-slice. DeepLesion reports the recall rate based on 2D image/CT-slice and the 3D box merging operation is not performed here.

**Table 2:** Results for our method and other detection methods averaged on the internal hold-out test sets from five datasets. Best in **bold**, second underline.

Model	Internal test						External test					
	Recall(%)@FPs					AP <sub>10</sub> <sup>box</sup>	Recall(%)@FPs					AP <sub>10</sub> <sup>box</sup>
	@0.5	@1	@2	@4	Avg.		@0.5	@1	@2	@4	Avg.	
Mask2Former	32.63	39.76	49.77	58.28	45.11	49.91	28.69	37.49	46.14	54.57	41.72	43.66
MP-Former	34.07	44.33	51.44	60.93	47.69	49.86	29.34	38.05	46.02	54.69	42.03	43.10
nnDetection	26.54	33.34	41.34	50.89	38.03	50.35	25.57	31.98	39.43	49.36	36.59	39.21
Mask-RCNN	31.24	37.05	49.21	60.33	44.45	46.63	27.00	34.52	47.87	53.46	40.71	42.18
LENS	33.55	43.84	54.17	<u>65.87</u>	49.36	<u>55.39</u>	26.83	36.52	44.42	53.62	40.35	45.55
MULAN	34.79	46.29	<u>57.75</u>	64.58	50.85	54.34	<u>34.99</u>	<u>44.36</u>	<u>53.00</u>	<u>59.80</u>	<u>48.03</u>	<u>47.43</u>
DINO	37.55	44.80	57.43	65.16	51.23	54.42	32.32	42.04	49.85	58.13	45.60	45.20
Mask DINO	<u>38.48</u>	<u>47.09</u>	55.27	64.43	<u>51.32</u>	54.72	34.80	43.05	51.49	58.20	46.89	46.90
<b>LN-DETR</b>	<b>42.48</b>	<b>51.02</b>	<b>60.60</b>	<b>70.96</b>	<b>56.27</b>	<b>58.47</b>	<b>35.26</b>	<b>48.18</b>	<b>57.92</b>	<b>66.78</b>	<b>52.04</b>	<b>50.24</b>
	+4.00%	+3.93%	+2.85%	+5.09%	+4.95%	+3.08%	+0.27%	+3.82%	+4.92%	+6.98%	+4.01%	+2.81%

**Comparing methods:** We conduct extensive comparison evaluation for LN detection, including the leading general object detection methods (Mask-RCNN [18], DINO [65] and Mask DINO [25]) and medical lesion detection methods (MULAN [60], LENS [58], nnDetection [3]), and two leading instance segmentation methods Mask2Former [9] and MP-Former [66]. For DeepLesion evaluation, methods reporting the leading testing results are compared [26, 27, 31, 51, 57, 58, 60].

**Implementation details:** We use ResNet-50 as the CNN backbone for feature extraction and adopt the same transformer configurations depicted in [25]. During training, we use a batch size of 8 with a starting learning rate of  $2e-4$ . Cosine learning rate scheduler is used to reduce the learning rate to  $1e-5$  with a warm-up step of 500. A weight decay of  $1e-4$  is set to avoid over-fitting. The models are trained for 30 epochs unless specified otherwise. We normalize the 3D CT volumes into a resolution of  $0.8 \times 0.8 \times 2\text{mm}$ , and randomly apply horizontal flipping, cropping, scaling, and random noise to augment the training data. The 2.5D fusion is adopted to all blocks in ResNet and the last three blocks' outputs are fed to the transformer encoder following [25]. We add position embedding and level embedding to the flattened tokens in the encoder, providing both spatial and level position priors. To generate initial content queries and anchor boxes after the encoder, we select the top 300 queries based on the proposed location debiased ranking criterion. In the decoder, we follow [25] to set the number of denoising queries as 100. During inference, we select the top 20 ranked query predictions as the final LN detection output.

## 4.2 Quantitative Results on LN Detection

**Comparison to other state-of-the-art Methods:** The quantitative performance of LN detection is summarized in Table 2 and some qualitative results are shown in Fig. 3. It can be observed that the proposed LN-DETR significantly outperforms other leading methods of different types in both internal and ex-

**Table 3:** Performance on the subgroup of *enlarged* lymph nodes.

Model	LN size $\geq 7$ mm					LN size $\geq 10$ mm				
	Recall(%)@FPs					Recall(%)@FPs				
	@0.5	@1	@2	@4	Avg.	@0.5	@1	@2	@4	Avg.
nnDetection	37.20	43.66	58.28	62.28	49.00	56.19	64.28	71.02	77.45	67.24
Mask2Former	45.84	53.53	63.58	68.51	57.87	57.48	64.01	73.06	76.39	67.74
MULAN	48.67	58.72	<u>67.64</u>	71.63	61.67	61.77	<u>71.70</u>	75.41	77.52	71.60
LENS	47.29	57.70	<u>67.21</u>	<u>75.45</u>	61.91	<u>62.20</u>	70.54	<u>76.94</u>	<u>82.06</u>	<u>72.94</u>
Mask DINO	<u>50.15</u>	<u>60.11</u>	67.50	72.48	<u>62.56</u>	60.36	70.59	76.46	80.63	72.01
<b>LN-DETR</b>	<b>56.35</b>	<b>63.96</b>	<b>71.70</b>	<b>77.04</b>	<b>67.26</b>	<b>67.29</b>	<b>76.99</b>	<b>80.81</b>	<b>83.50</b>	<b>77.15</b>

ternal testing. LN-DETR achieves an average recall of 56.27% across 0.5 to 4 FPs/patient in the **internal testing**, which is markedly higher than the second best performing method of original Mask DINO [25] with a margin of 4.95%. When compared to other popular or representative universal lesion detection methods MULAN [60], LENS [58] and nnDetection [3], LN-DETR increases the average recall by 5.42%, 6.91% and 18.24%, respectively. It is worth noting that LN detection-by-segmentation generally yields inferior performance (although with longer training epochs) as compared to direct detection methods. For example, two state-of-the-art instance segmentation methods Mask2Former [9] and MP-Former [66] only obtain 45.11% and 47.69% average recall, respectively.

For the **external testing**, LN-DETR generalizes well as shown in Table 2. LN-DETR achieves an average recall of 52.04% across 0.5 to 4 FPs/patient outperforming the second best performing method of MULAN [60] by 4.01%. Original Mask DINO obtains a slightly decreased recall as compared to MULAN (46.89% vs. 48.03%). This demonstrates that directly applying the state-of-the-art detection transformers may not yield better performance as compared to specifically designed and adapted CNN-based models (like MULAN). Among the comparing methods, LENS [58] experiences the most markedly performance drop when generalizing to the external testing (from 49.36% to 40.35%). A similar trend is evident in AP evaluation, with improvements of 3.08% and 2.81% internally and externally, respectively, compared to the closest competitor.

**Performance on the subgroup of enlarged LNs:** We also examine the subgroup performance by reporting the LN detection results on LNs  $\geq 7$ mm and  $\geq 10$ mm, respectively. Results are summarized in Table 3. We observe that LN-DETR performs consistently across different LN sizes, as it maintains about 5% improvement to the second best method for LNs  $\geq 7$ mm,  $\geq 10$ mm, and all sizes. It is also noted that for enlarged LNs  $\geq 10$ mm, LN-DETR reports a recall of 83.5% at 4FPs per patient. In contrast, previous works often report quite lower performance. For instance, 60.9% recall at 6.1FPs/patient [16] is reported in the chest region, and 73.9% at 9FPs/patient are reported in the abdomen region [54].

**Ablation Results:** The effectiveness of three components in LN-DETR, *i.e.*, 2.5D feature fusion, location debiased query selection and query contrastive

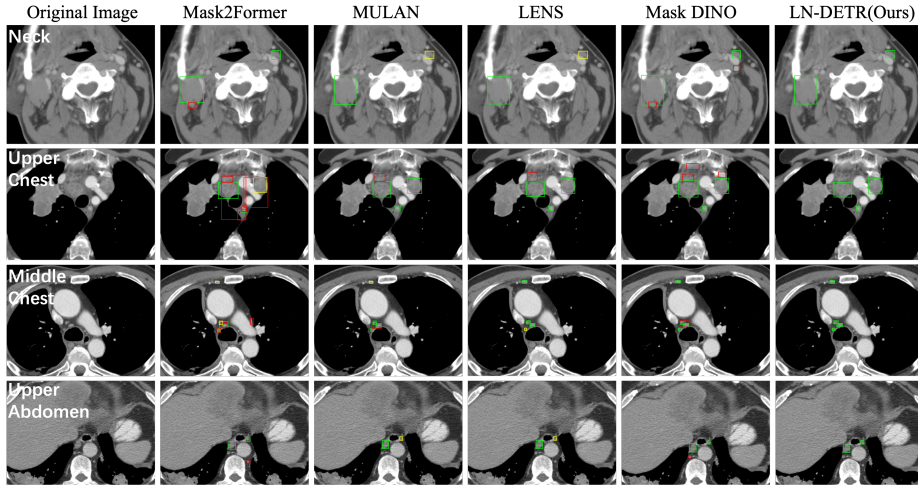


**Fig. 3:** Qualitative comparisons with other leading detection methods on different body parts, from neck to upper abdomen. **Green**, **red**, and **yellow** denote for TP, FP and FN, respectively. Compared to previous CNN-based detection methods (*e.g.*, MULAN and LENS), our method exhibits higher sensitivity. Additionally, we have significantly reduced false positive predictions of Mask DINO.

**Table 4:** Ablation results of the effectiveness of the proposed multi-scale 2.5D fusion, debiased query selection (DQS), and contrastive learning (CL).

2.5D	CL	DQS	Recall(%)@FPs				Avg.
			@0.5	@1	@2	@4	
			38.48	47.09	55.27	64.43	51.32
✓			39.34	48.24	56.07	65.96	52.40 (+1.08%)
✓	✓		39.28	48.62	58.40	67.46	53.44 (+2.12%)
✓		✓	40.96	48.90	59.24	68.93	54.51 (+3.19%)
✓	✓	✓	42.48	51.02	60.60	70.96	<b>56.27 (+4.95%)</b>

learning, are demonstrated in ablation Table 4. First, the 2.5D feature fusion increases the performance by 1.08% average recall across 0.5 to 4 FPs/patient as compared to the plain 2D Mask DINO (from 51.32% to 52.40%). Based on the 2.5D fusion, query contrastive learning and debiased query selection alone can improve the average recall of LN detection by 1.04% (from 52.40% to 53.44%) and 2.11% (from 52.40% to 54.51%), respectively. More importantly, combining these two modules, our final LN-DETR significantly boosts the average recall by almost 4%. Due to space limits, other ablation results are reported in the supplementary materials, such as the selection of temperature  $\tau$  for query contrastive learning, loss weight for  $\mathcal{L}_{IoU}$ , and LN instance segmentation performance comparison using the metric of mask AP [25].

**Table 5:** Quantitative results on NIH DeepLesion testing dataset. P3D\* is pre-trained using MS-COCO, and performance would be decreased when using ImageNet pretraining. In contrast, our method uses the ImageNet pre-trained backbone.

Methods	Recall(%)@FPs				Avg.
	@0.5	@1	@2	@4	
A3D	79.24	85.04	89.15	92.71	86.54
LENS	78.60	85.50	89.60	92.50	86.60
DKMA	78.48	85.95	90.48	93.48	87.16
A3D+SATr	<u>81.03</u>	86.64	90.70	93.30	87.92
DiffULD	80.43	<u>87.16</u>	91.20	93.21	88.00
P3D*	<b>82.22</b>	<b>87.42</b>	<u>90.91</u>	<u>93.65</u>	<b>88.55</b>
<b>LN-DETR</b>	79.89	87.05	<b>92.00</b>	<b>94.89</b>	<u>88.46</u>

### 4.3 Quantitative Results on NIH DeepLesion Benchmark

Detailed results on the official testing set of DeepLesion are summarized in Table 5. We compare our LN-DETR to the leading methods in the universal lesion detection task. As shown in the table, our proposed LN-DETR achieves top-performing results with an 88.46% average recall across 0.5 to 4 FPs/image (comparable to P3D\* using MS-COCO pre-trained backbone). Notably, LN-DETR obtains similar or even higher recall rate with 2 FPs/image as compared to several methods with doubled 4 FPs (92.00% vs. 85.65% [57], 90.77% [72], 91.30% [31], 92.30% [60]). When considering the recall rate at four FPs/image, our method achieves a recall rate of  $\sim 95\%$ , significantly higher than all prior arts by a noticeable margin. As can be seen, our method demonstrates the superior generalization ability on a different detection task in CT images.

## 5 Conclusion

In this work, we tackle the critical yet challenging task of lymph node detection. Building on the latest transformer detection/segmentation framework Mask DINO, we propose a new LN detection transformer, LN-DETR, to achieve more accurate performance. We introduce a location debiased query selection of higher localization accuracy as decoder query’s initialization and a query contrastive learning module to improve the learned query quality and reduce the false positive and duplicated predictions. Trained and tested on 3D CT scans of 1067 patients with 10,000+ labeled LNs (largest LN dataset to date), our method significantly improves the previous leading LN detection methods by at least 4  $\sim$  5% average recall in both internal and external testing. When further evaluated on the universal lesion detection task using DeepLesion, LN-DETR achieves the top performance of 88.46% recall.

## References

1. Ardila, D., Kiraly, A.P., Bharadwaj, S., Choi, B., Reicher, J.J., Peng, L., Tse, D., Etemadi, M., Ye, W., Corrado, G., et al.: End-to-end lung cancer screening with three-dimensional deep learning on low-dose chest computed tomography. *Nature medicine* **25**(6), 954–961 (2019)
2. Barbu, A., Suehling, M., Xu, X., Liu, D., Zhou, S.K., Comaniciu, D.: Automatic detection and segmentation of lymph nodes from ct data. *IEEE Transactions on Medical Imaging* **31**(2), 240–250 (2011)
3. Baumgartner, M., Jäger, P.F., Isensee, F., Maier-Hein, K.H.: nndetection: a self-configuring method for medical object detection. In: *Medical Image Computing and Computer Assisted Intervention–MICCAI*. pp. 530–539. Springer (2021)
4. Bouget, D., Jørgensen, A., Kiss, G., Leira, H.O., Langø, T.: Semantic segmentation and detection of mediastinal lymph nodes and anatomical structures in ct data for lung cancer staging. *International journal of computer assisted radiology and surgery* **14**, 977–986 (2019)
5. Bouget, D., Pedersen, A., Vanel, J., Leira, H.O., Langø, T.: Mediastinal lymph nodes segmentation using 3d convolutional neural network ensembles and anatomical priors guiding. *Computer Methods in Biomechanics and Biomedical Engineering: Imaging & Visualization* **11**(1), 44–58 (2023)
6. Carion, N., Massa, F., Synnaeve, G., Usunier, N., Kirillov, A., Zagoruyko, S.: End-to-end object detection with transformers. In: *European conference on computer vision*. pp. 213–229. Springer (2020)
7. Chang, J.M., Leung, J.W., Moy, L., Ha, S.M., Moon, W.K.: Axillary nodal evaluation in breast cancer: state of the art. *Radiology* **295**(3), 500–515 (2020)
8. Chen, T., Kornblith, S., Norouzi, M., Hinton, G.: A simple framework for contrastive learning of visual representations. In: *International conference on machine learning*. pp. 1597–1607. PMLR (2020)
9. Cheng, B., Misra, I., Schwing, A.G., Kirillov, A., Girdhar, R.: Masked-attention mask transformer for universal image segmentation. In: *Proceedings of the IEEE/CVF conference on computer vision and pattern recognition*. pp. 1290–1299 (2022)
10. Cheng, C.T., Wang, Y., Chen, H.W., Hsiao, P.M., Yeh, C.N., Hsieh, C.H., Miao, S., Xiao, J., Liao, C.H., Lu, L.: A scalable physician-level deep learning algorithm detects universal trauma on pelvic radiographs. *Nature communications* **12**(1), 1066 (2021)
11. Chilamkurthy, S., Ghosh, R., Tanamala, S., Biviji, M., Campeau, N.G., Venugopal, V.K., Mahajan, V., Rao, P., Warier, P.: Deep learning algorithms for detection of critical findings in head ct scans: a retrospective study. *The Lancet* **392**(10162), 2388–2396 (2018)
12. Detterbeck, F.C., Boffa, D.J., Kim, A.W., Tanoue, L.T.: The eighth edition lung cancer stage classification. *Chest* **151**(1), 193–203 (2017)
13. Dosovitskiy, A., Beyer, L., Kolesnikov, A., Weissenborn, D., Zhai, X., Unterthiner, T., Dehghani, M., Minderer, M., Heigold, G., Gelly, S., et al.: An image is worth 16x16 words: Transformers for image recognition at scale. *arXiv preprint arXiv:2010.11929* (2020)
14. El-Sherief, A.H., Lau, C.T., Wu, C.C., Drake, R.L., Abbott, G.F., Rice, T.W.: International association for the study of lung cancer (iaslc) lymph node map: radiologic review with ct illustration. *Radiographics* **34**(6), 1680–1691 (2014)

15. Feuerstein, M., Glocker, B., Kitasaka, T., Nakamura, Y., Iwano, S., Mori, K.: Mediastinal atlas creation from 3-d chest computed tomography images: application to automated detection and station mapping of lymph nodes. *Medical image analysis* **16**(1), 63–74 (2012)
16. Feulner, J., Zhou, S.K., Hammon, M., Hornegger, J., Comaniciu, D.: Lymph node detection and segmentation in chest ct data using discriminative learning and a spatial prior. *Medical image analysis* **17**(2), 254–270 (2013)
17. Guo, D., Ge, J., Yan, K., Wang, P., Zhu, Z., Zheng, D., Hua, X.S., Lu, L., Ho, T.Y., Ye, X., et al.: Thoracic lymph node segmentation in ct imaging via lymph node station stratification and size encoding. In: *International Conference on Medical Image Computing and Computer-Assisted Intervention*. pp. 55–65. Springer (2022)
18. He, K., Gkioxari, G., Dollár, P., Girshick, R.: Mask r-cnn. In: *Proceedings of the IEEE international conference on computer vision*. pp. 2961–2969 (2017)
19. Jia, D., Yuan, Y., He, H., Wu, X., Yu, H., Lin, W., Sun, L., Zhang, C., Hu, H.: Detsr with hybrid matching. In: *Proceedings of the IEEE/CVF Conference on Computer Vision and Pattern Recognition*. pp. 19702–19712 (2023)
20. Jiang, B., Luo, R., Mao, J., Xiao, T., Jiang, Y.: Acquisition of localization confidence for accurate object detection. In: *Proceedings of the European conference on computer vision (ECCV)*. pp. 784–799 (2018)
21. Kann, B.H., Hicks, D.F., Payabvash, S., Mahajan, A., Du, J., Gupta, V., Park, H.S., Yu, J.B., Yarbrough, W.G., Burtness, B.A., et al.: Multi-institutional validation of deep learning for pretreatment identification of extranodal extension in head and neck squamous cell carcinoma. *Journal of Clinical Oncology* **38**(12), 1304–1311 (2020)
22. Khosla, P., Teterwak, P., Wang, C., Sarna, A., Tian, Y., Isola, P., Maschinot, A., Liu, C., Krishnan, D.: Supervised contrastive learning. *Advances in neural information processing systems* **33**, 18661–18673 (2020)
23. Kuhn, H.W.: The hungarian method for the assignment problem. *Naval research logistics quarterly* **2**(1-2), 83–97 (1955)
24. Li, F., Zhang, H., Liu, S., Guo, J., Ni, L.M., Zhang, L.: Dn-detr: Accelerate detr training by introducing query denoising. In: *Proceedings of the IEEE/CVF Conference on Computer Vision and Pattern Recognition*. pp. 13619–13627 (2022)
25. Li, F., Zhang, H., Xu, H., Liu, S., Zhang, L., Ni, L.M., Shum, H.Y.: Mask dino: Towards a unified transformer-based framework for object detection and segmentation. In: *Proceedings of the IEEE/CVF Conference on Computer Vision and Pattern Recognition*. pp. 3041–3050 (2023)
26. Li, H., Chen, L., Han, H., Chi, Y., Zhou, S.K.: Conditional training with bounding map for universal lesion detection. In: *International Conference on Medical Image Computing and Computer-Assisted Intervention*. pp. 141–152. Springer (2021)
27. Li, H., Chen, L., Han, H., Kevin Zhou, S.: Satr: Slice attention with transformer for universal lesion detection. In: *International Conference on Medical Image Computing and Computer-Assisted Intervention*. pp. 163–174. Springer (2022)
28. Li, J., Dai, H., Shao, L., Ding, Y.: From voxel to point: Iou-guided 3d object detection for point cloud with voxel-to-point decoder. In: *Proceedings of the 29th ACM International Conference on Multimedia*. pp. 4622–4631 (2021)
29. Li, J., Chen, J., Tang, Y., Wang, C., Landman, B.A., Zhou, S.K.: Transforming medical imaging with transformers? a comparative review of key properties, current progresses, and future perspectives. *Medical image analysis* p. 102762 (2023)
30. Li, X., Wang, W., Wu, L., Chen, S., Hu, X., Li, J., Tang, J., Yang, J.: Generalized focal loss: Learning qualified and distributed bounding boxes for dense object

- detection. *Advances in Neural Information Processing Systems* **33**, 21002–21012 (2020)
31. Li, Z., Zhang, S., Zhang, J., Huang, K., Wang, Y., Yu, Y.: Mvp-net: multi-view fpn with position-aware attention for deep universal lesion detection. In: *Medical Image Computing and Computer Assisted Intervention–MICCAI*. pp. 13–21. Springer (2019)
  32. Lin, T.Y., Dollár, P., Girshick, R., He, K., Hariharan, B., Belongie, S.: Feature pyramid networks for object detection. In: *Proceedings of the IEEE conference on computer vision and pattern recognition*. pp. 2117–2125 (2017)
  33. Liu, J., Hoffman, J., Zhao, J., Yao, J., Lu, L., Kim, L., Turkbey, E.B., Summers, R.M.: Mediastinal lymph node detection and station mapping on chest ct using spatial priors and random forest. *Medical physics* **43**(7), 4362–4374 (2016)
  34. Liu, S., Li, F., Zhang, H., Yang, X., Qi, X., Su, H., Zhu, J., Zhang, L.: Dab-detr: Dynamic anchor boxes are better queries for detr. *arXiv preprint arXiv:2201.12329* (2022)
  35. Long, J., Shelhamer, E., Darrell, T.: Fully convolutional networks for semantic segmentation. In: *Proceedings of the IEEE conference on computer vision and pattern recognition*. pp. 3431–3440 (2015)
  36. Mathai, T.S., Lee, S., Elton, D.C., Shen, T.C., Peng, Y., Lu, Z., Summers, R.M.: Detection of lymph nodes in t2 mri using neural network ensembles. In: *Machine Learning in Medical Imaging: 12th International Workshop*. pp. 682–691. Springer (2021)
  37. McCloud, T., Bourgouin, P., Greenberg, R., Kosiuk, J., Templeton, P., Shepard, J.A., Moore, E., Wain, J., Mathisen, D., Grillo, H.: Bronchogenic carcinoma: analysis of staging in the mediastinum with ct by correlative lymph node mapping and sampling. *Radiology* **182**(2), 319–323 (1992)
  38. Meng, D., Chen, X., Fan, Z., Zeng, G., Li, H., Yuan, Y., Sun, L., Wang, J.: Conditional detr for fast training convergence. In: *Proceedings of the IEEE/CVF International Conference on Computer Vision*. pp. 3651–3660 (2021)
  39. Mitani, A., Huang, A., Venugopalan, S., Corrado, G.S., Peng, L., Webster, D.R., Hammel, N., Liu, Y., Varadarajan, A.V.: Detection of anaemia from retinal fundus images via deep learning. *Nature Biomedical Engineering* **4**(1), 18–27 (2020)
  40. Mountain, C.F., Dresler, C.M.: Regional lymph node classification for lung cancer staging. *Chest* **111**(6), 1718–1723 (1997)
  41. Oda, H., Roth, H.R., Bhatia, K.K., Oda, M., Kitasaka, T., Iwano, S., Homma, H., Takabatake, H., Mori, M., Natori, H., et al.: Dense volumetric detection and segmentation of mediastinal lymph nodes in chest ct images. In: *Medical Imaging 2018: Computer-Aided Diagnosis*. vol. 10575, p. 1057502. SPIE (2018)
  42. Oord, A.v.d., Li, Y., Vinyals, O.: Representation learning with contrastive predictive coding. *arXiv preprint arXiv:1807.03748* (2018)
  43. Pu, Y., Liang, W., Hao, Y., Yuan, Y., Yang, Y., Zhang, C., Hu, H., Huang, G.: Rank-detr for high quality object detection. *Advances in Neural Information Processing Systems* **36** (2024)
  44. Redmon, J., Farhadi, A.: Yolo9000: better, faster, stronger. In: *Proceedings of the IEEE conference on computer vision and pattern recognition*. pp. 7263–7271 (2017)
  45. Redmon, J., Farhadi, A.: Yolov3: An incremental improvement. *arXiv preprint arXiv:1804.02767* (2018)
  46. Ren, S., He, K., Girshick, R., Sun, J.: Faster r-cnn: Towards real-time object detection with region proposal networks. *Advances in neural information processing systems* **28** (2015)

47. Rice, T.W., Ishwaran, H., Ferguson, M.K., Blackstone, E.H., Goldstraw, P.: Cancer of the esophagus and esophagogastric junction: an eighth edition staging primer. *Journal of Thoracic Oncology* **12**(1), 36–42 (2017)
48. Roth, H.R., Lu, L., Liu, J., Yao, J., Seff, A., Cherry, K., Kim, L., Summers, R.M.: Improving computer-aided detection using convolutional neural networks and random view aggregation. *IEEE transactions on medical imaging* **35**(5), 1170–1181 (2015)
49. Schwartz, L., Bogaerts, J., Ford, R., Shankar, L., Therasse, P., Gwyther, S., Eisenhauer, E.: Evaluation of lymph nodes with recist 1.1. *European journal of cancer* **45**(2), 261–267 (2009)
50. Shamshad, F., Khan, S., Zamir, S.W., Khan, M.H., Hayat, M., Khan, F.S., Fu, H.: Transformers in medical imaging: A survey. *Medical Image Analysis* p. 102802 (2023)
51. Sheoran, M., Dani, M., Sharma, M., Vig, L.: Dkma-uld: domain knowledge augmented multi-head attention based robust universal lesion detection. *arXiv preprint arXiv:2203.06886* (2022)
52. Takeuchi, H., Fujii, H., Ando, N., Ozawa, S., Saikawa, Y., Suda, K., Oyama, T., Mukai, M., Nakahara, T., Kubo, A., et al.: Validation study of radio-guided sentinel lymph node navigation in esophageal cancer. *Annals of surgery* **249**(5), 757–763 (2009)
53. Tian, Z., Shen, C., Chen, H., He, T.: Fcos: Fully convolutional one-stage object detection. In: *Proceedings of the IEEE/CVF international conference on computer vision*. pp. 9627–9636 (2019)
54. Wang, S., Zhu, Y., Lee, S., Elton, D.C., Shen, T.C., Tang, Y., Peng, Y., Lu, Z., Summers, R.M.: Global-local attention network with multi-task uncertainty loss for abnormal lymph node detection in mr images. *Medical Image Analysis* **77**, 102345 (2022)
55. Wang, Y., Zhang, X., Yang, T., Sun, J.: Anchor detr: Query design for transformer-based detector. In: *Proceedings of the AAAI conference on artificial intelligence*. vol. 36, pp. 2567–2575 (2022)
56. Wu, C., Chang, F., Su, X., Wu, Z., Wang, Y., Zhu, L., Zhang, Y.: Integrating features from lymph node stations for metastatic lymph node detection. *Computerized Medical Imaging and Graphics* **101**, 102108 (2022)
57. Yan, K., Bagheri, M., Summers, R.M.: 3d context enhanced region-based convolutional neural network for end-to-end lesion detection. In: *Medical Image Computing and Computer Assisted Intervention–MICCAI*. pp. 511–519. Springer (2018)
58. Yan, K., Cai, J., Zheng, Y., Harrison, A.P., Jin, D., Tang, Y., Tang, Y., Huang, L., Xiao, J., Lu, L.: Learning from multiple datasets with heterogeneous and partial labels for universal lesion detection in ct. *IEEE Transactions on Medical Imaging* **40**(10), 2759–2770 (2021)
59. Yan, K., Jin, D., Guo, D., Xu, M., Shen, N., Hua, X.S., Ye, X., Lu, L.: Anatomy-aware lymph node detection in chest ct using implicit station stratification. *arXiv preprint arXiv:2307.15271* (2023)
60. Yan, K., Tang, Y., Peng, Y., Sandfort, V., Bagheri, M., Lu, Z., Summers, R.M.: Mulan: multitask universal lesion analysis network for joint lesion detection, tagging, and segmentation. In: *Medical Image Computing and Computer Assisted Intervention–MICCAI*. pp. 194–202. Springer (2019)
61. Yan, K., Wang, X., Lu, L., Summers, R.M.: Deeplesion: automated mining of large-scale lesion annotations and universal lesion detection with deep learning. *Journal of medical imaging* **5**(3), 036501–036501 (2018)

62. Yang, J., He, Y., Kuang, K., Lin, Z., Pfister, H., Ni, B.: Asymmetric 3d context fusion for universal lesion detection. In: *Medical Image Computing and Computer Assisted Intervention–MICCAI*. pp. 571–580. Springer (2021)
63. Yao, Z., Ai, J., Li, B., Zhang, C.: Efficient detr: improving end-to-end object detector with dense prior. arXiv preprint arXiv:2104.01318 (2021)
64. Ye, M., Ke, L., Li, S., Tai, Y.W., Tang, C.K., Danelljan, M., Yu, F.: Cascade-detr: Delving into high-quality universal object detection. In: *Proceedings of the IEEE/CVF International Conference on Computer Vision*. pp. 6704–6714 (2023)
65. Zhang, H., Li, F., Liu, S., Zhang, L., Su, H., Zhu, J., Ni, L.M., Shum, H.Y.: Dino: Detr with improved denoising anchor boxes for end-to-end object detection. arXiv preprint arXiv:2203.03605 (2022)
66. Zhang, H., Li, F., Xu, H., Huang, S., Liu, S., Ni, L.M., Zhang, L.: Mp-former: Mask-piloted transformer for image segmentation. In: *Proceedings of the IEEE/CVF Conference on Computer Vision and Pattern Recognition*. pp. 18074–18083 (2023)
67. Zhang, H., Wang, Y., Dayoub, F., Sunderhauf, N.: Varifocalnet: An iou-aware dense object detector. In: *Proceedings of the IEEE/CVF conference on computer vision and pattern recognition*. pp. 8514–8523 (2021)
68. Zhang, S., Li, Z., Zhou, H.Y., Ma, J., Yu, Y.: Advancing 3d medical image analysis with variable dimension transform based supervised 3d pre-training. *Neurocomputing* **529**, 11–22 (2023)
69. Zhu, X., Su, W., Lu, L., Li, B., Wang, X., Dai, J.: Deformable detr: Deformable transformers for end-to-end object detection. arXiv preprint arXiv:2010.04159 (2020)
70. Zhu, Z., Jin, D., Yan, K., Ho, T.Y., Ye, X., Guo, D., Chao, C.H., Xiao, J., Yuille, A., Lu, L.: Lymph node gross tumor volume detection and segmentation via distance-based gating using 3d ct/pet imaging in radiotherapy. In: *International Conference on Medical Image Computing and Computer-Assisted Intervention*. pp. 753–762. Springer (2020)
71. Zhu, Z., Yan, K., Jin, D., Cai, J., Ho, T.Y., Harrison, A.P., Guo, D., Chao, C.H., Ye, X., Xiao, J., et al.: Detecting scatteredly-distributed, small, andcritically important objects in 3d oncologyimaging via decision stratification. arXiv preprint arXiv:2005.13705 (2020)
72. Zlocha, M., Dou, Q., Glocker, B.: Improving retinanet for ct lesion detection with dense masks from weak recist labels. In: *Medical Image Computing and Computer Assisted Intervention–MICCAI 2019: 22nd International Conference, Shenzhen, China, October 13–17, 2019, Proceedings, Part VI 22*. pp. 402–410. Springer (2019)